

LiDAR-Based Detection of Urban Trees Using a Backpack System

Matheus Ferreira da Silva¹, Leticia Ferrari Castanheiro¹, Antonio Maria Garcia Tommaselli^{1,2}, Renato César dos Santos^{1,2},
Mauricio Galo^{1,2}

¹ Graduate Program in Cartographic Sciences, São Paulo State University (UNESP), Presidente Prudente, São Paulo, Brazil
{matheus-ferreira.silva, leticia.ferrari}@unesp.br

² Department of Cartography, São Paulo State University (UNESP), Presidente Prudente, São Paulo, Brazil
{a.tommaselli, renato.cesar, mauricio.galo}@unesp.br

Keywords: GSW 2025, 3D Mapping, Mobile LASER Scanning, Urban Forests, Tree Location, Vertical Continuity.

Abstract

Mapping individual trees accurately in densely populated urban environments is challenging due to occlusion effects, overlapping canopies, and irregular tree morphology. This paper presents and evaluates an automated tree detection technique based on the vertical continuity principle to decrease the reliance on preprocessing steps, such as terrain filtering and point cloud normalization. A heuristic filter effectively distinguishes trees from pole-like structures that demonstrate vertical continuity, which helps to reduce false positives. Data were collected using a backpack LiDAR (Light Detection and Ranging) system with an accuracy of 5 cm. The sensor's effective range is up to 50 m (at 80% reflectivity), enabling the acquisition of high-density point clouds at close-range distances while maintaining efficiency and accessibility in complex urban environments. The method was tested across three diverse urban sites, with 156 trees, and achieved an F_{Score} of 94.1%, with a 26 cm horizontal RMSE_{XY} in trunk positioning.

1. Introduction

Urban forest mapping is critical for sustainable development, as vegetation provides many ecological, social, and economic benefits to urban environments (Hu et al., 2022). The rapid urban expansion observed in recent decades has resulted in an uneven distribution of vegetation, characterized by the rise in impermeable surfaces, such as concrete, and the removal of trees. These alterations to the urban landscape directly contribute to the formation of heat islands, promoting microclimate variations, air quality degradation, noise pollution, and a decline in social well-being (Lee et al., 2024). Effective urban vegetation management is required to address these challenges, beginning with the identification of areas with inadequate vegetation cover. Then, quantitative parameters, including geographical tree location, health conditions, and morphological attributes such as crown diameter, diameter at breast height (DBH), and height (Dalla Corte et al., 2020), are extracted to characterize the urban forest structure. These parameters enable public authorities to develop strategies to manage and implement interventions for a more equitable distribution of green spaces.

Traditional data collection methods, mainly manual surveys, pose significant challenges due to the high costs of mapping large-scale areas. This frequently leads to the production of incomplete datasets, thereby hindering effective urban planning management. Remote sensing technologies, particularly Light Detection and Ranging (LiDAR), have emerged as an alternative for mapping urban forests, given their capacity to acquire high-resolution data over expansive areas (Neyns and Canters, 2022). LiDAR systems capture detailed three-dimensional (3D) point cloud data, allowing the extraction of structural information such as trunk shape, branches, and canopy boundaries (da Silva et al., 2023; Yang et al., 2024), which would be impractical to obtain through conventional methods.

LiDAR's derived information extends beyond basic tree inventories, including estimating biomass and carbon stocks to calculate green cover indexes, contributing to urban analytical

planning (Bergmann et al., 2024). Furthermore, LiDAR data enables the analysis of vegetation conflicts with infrastructure (e.g., buildings, roads, and power lines). Urban planning regulations often guide these diverse applications, including species restrictions, maximum height limitations, and road clearance requirements (Carnot et al., 2024).

The efficiency of LiDAR-based approaches depends on the strategies employed for tree detection and localization. These approaches can generally be divided into three principal categories: classical rule-based, machine learning (ML), and deep learning (DL). Classical techniques rely on well-defined parameters in mathematics models. Circle fitting is frequently employed to model the cross-sections of trunks (Wu et al., 2018), whereas cylinder fitting is utilized to represent entire trunks (Ma et al., 2025). Nevertheless, establishing appropriate parameters within this domain presents significant challenges, often requiring extensive fine-tuning (Dos Santos, Da Silva, Alencar et al., 2024; Yao et al., 2014). ML strategies rely on labeled datasets and local geometric descriptors extracted from the point cloud to differentiate trunks from other objects. This dependence on annotated data and handcrafted features may limit their adaptability. Although DL approaches can autonomously extract features from point clouds, large amounts of labeled data are required. Moreover, they face challenges associated with contextual variations in point density, noise, and the efficient processing of large datasets (Kulicki et al., 2024).

Despite the great set of methodologies, many existing methods remain limited by their dependence on extensive parameter fine-tuning and substantial preprocessing steps, such as terrain filtering and point cloud normalization (Hui et al., 2022; Husain & Vaishya, 2019; Ma et al., 2025; Solares-Canal et al., 2023; Wang et al., 2020). This dependency can limit adaptability to the irregular and fragmented tree canopies in urban environments. To overcome this limitation, this paper proposes a tree detection approach based on the vertical continuity of tree trunks. The main contributions of our work are as follows:

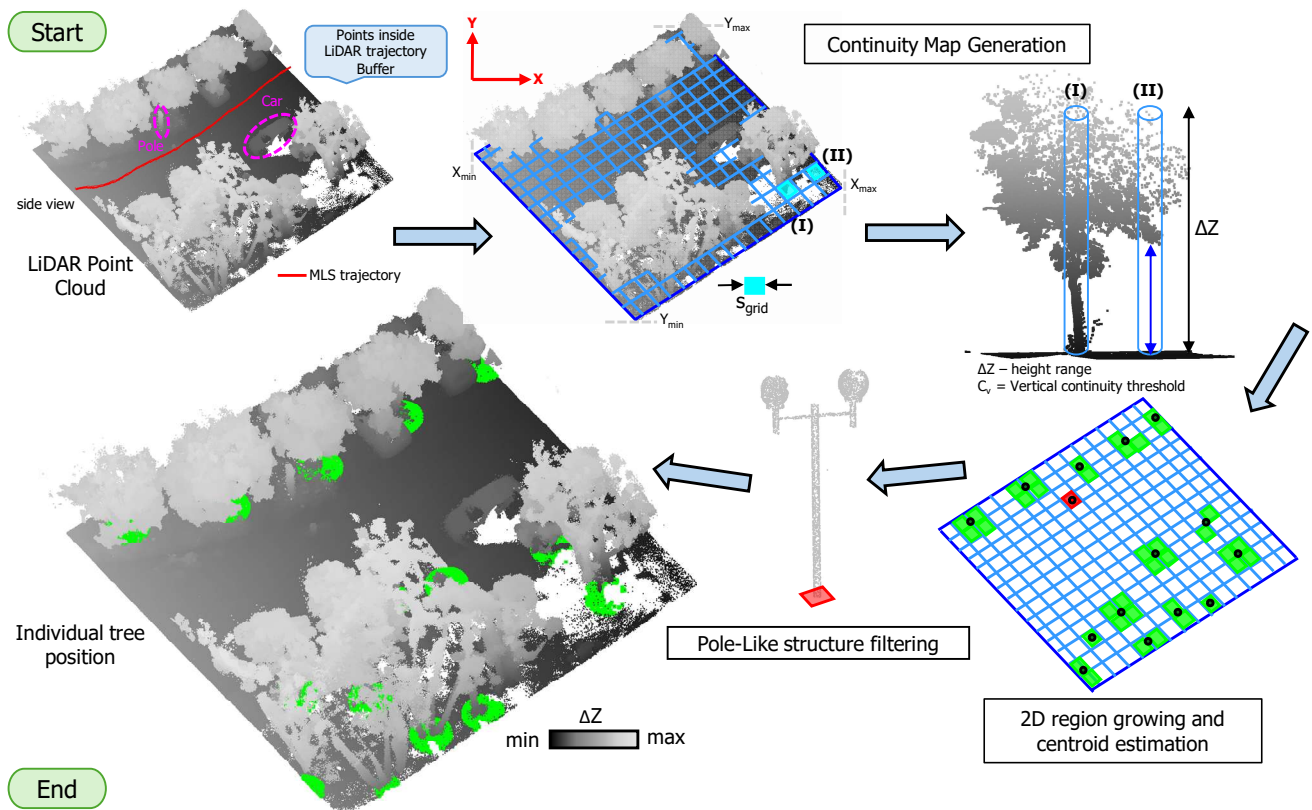


Figure 1. Flowchart of the tree detection method using vertical continuity analysis.

- Development of an automatic tree detection approach using trunk point sampling to accurately identify individual trees in urban environments where crowns often overlap or fragment.
- Explore the use of a straightforward continuity map derived from the raw point cloud to simplify the detection process and enhance robustness against variations in vegetation structures.
- Reducing the requirements for pre-processing, including filtering, point cloud normalization, and classification.
- Propose an automatic strategy to eliminate non-tree objects, such as pole-like structures, which typically exhibit strong vertical continuity.

2. Related works

LiDAR systems can be employed across various platforms (aerials and terrestrials), each suited for distinct scales and levels of detail. Aerial platforms, such as Airborne Laser Scanning (ALS) and Unmanned Aerial Vehicles (UAVs), are ideal for large-scale canopy mapping (Yang et al., 2024), but the resolution may lack the level of detail needed for urban forest analysis. In contrast, terrestrial systems, including Terrestrial Laser Scanning (TLS) and Mobile Laser Scanning (MLS) systems, provide more details of individual tree characteristics at ground-level mapping (Luo et al., 2021). Among terrestrial platforms, TLS offers high-precision and detailed 3D models. However, its fixed configuration and the need for multiple scans from different TLS station positions make it costly and time-consuming for large-scale coverage (Shao et al., 2020), limiting its application in urban forest mapping. Conversely, MLS combined the mobility of ALS with

the terrestrial perspective of TLS, achieving a balance between cost and efficiency; however, it is comparatively less accurate than TLS and is more susceptible to noise and outliers due to its mobile data collection.

Luo et al. (2021) proposed a novel top-down approach to extract individual trees from urban MLS point clouds. Their method involves applying a semantic segmentation deep network to identify tree points from raw MLS data, then grouping them into clusters using Euclidean distance clustering. They introduced a pointwise direction embedding deep network (PDE-net) to predict direction vectors pointing to tree centers, enhancing the boundaries of instance-level trees. This approach achieved precision, recall, and F_{Score} of 96%, 94%, and 95%, respectively. However, the process of tree center detection involves an empirical threshold (N_d) for the number of direction rays, which may limit the method's generalization ability. Additionally, some separation errors at the boundaries of instance-level trees were observed.

Takahashi and Masuda (2021) proposed a method for detecting roadside trees and automatically estimating their diameters at breast height from MLS point clouds. Their approach maps point clouds onto a 2D image plane, converting them into a wireframe model and calculating geometric features for each point. Tree points are detected using machine learning techniques, and the DBH of each tree is calculated using vertically aligned circles extracted from the wireframe model. This method performed extraction with an F_{Score} of 97.49% for 102 roadside trees. However, challenges remain, particularly in instances where multiple trees are treated as a single object.

Kou et al. (2025) propose an algorithm for roadside tree segmentation and parameter extraction. The method addresses common challenges associated with point cloud data collected with MLS, including missing points caused by interference

from surrounding objects, which can lead to over-segmentation and under-segmentation. The process begins with segmenting the tree scene using the DBSCAN (Density-Based Spatial Clustering of Applications with Noise) algorithm. Then, the results are optimized, ensuring effective segmentation through projection topology checking and tree-adaptive voxel boundary analysis. The final step extracts key tree parameters such as height, DBH, and crown area. Experimental results show an average segmentation accuracy of 99.07% and a parameter extraction accuracy exceeding 90%.

3. Tree Detection Approach

3.1 Point Cloud Preprocessing Stage

Data preprocessing focused on filtering the raw point clouds to retain only close-range points to the operator's trajectory, assuming those are the most relevant for tree detection. A buffer area (B_A) was applied around the MLS trajectory to define the region of interest. This filtering reduces computational load and eliminates irrelevant data, such as partially mapped building facades and edge vegetation.

3.2 Detection of Vertically Continuous Objects

The detection of vertically continuous objects (Dos Santos, Da Silva, Tommaselli, et al., 2024), a critical step for identifying tree trunks, begins by superimposing a regular grid over the area of interest (XY_{min} ; XY_{max}). Each grid cell has dimensions $s_{grid} \times s_{grid}$, where s_{grid} corresponds to the diameter of the smallest detectable tree trunk. This cell size ensures that every trunk cross-section with a diameter greater than s_{grid} is analyzed.

For each grid cell, neighboring LiDAR points are evaluated within a vertical cylinder of radius $s_{grid}/2$. The cylinder extends vertically from Z_{min} (the local minimum height within the cell) to $Z_{max} = Z_{min} + \Delta Z$, where ΔZ represents the minimum trunk height of interest. Points within the cylinder are sorted in ascending order based on their Z-coordinate, generating a height vector $V = \{z_1, z_2, \dots, z_n\}$ that isolates potential trunk points.

Vertical continuity is assessed by calculating the vertical differences between consecutive points in vector V (Equation 1):

$$\Delta Z_i = Z_{i+1} - Z_i, \text{ for } i = 1, 2, \dots, n - 1 \quad (1)$$

A grid cell is considered a trunk candidate only if all ΔZ_i values are smaller than the vertical continuity threshold c_v , defined based on the vertical point spacing. This criterion filters out fragmented structures (e.g., shrubs, noise points) that exhibit discontinuous vertical profiles.

Adjacent trunk candidate cells are aggregated using an 8-connected region-growing algorithm to delineate individual trees. Tree trunk position (X_c, Y_c) is computed as the centroid of the grouped cell. The flowchart shown in Figure 1 illustrates the details.

3.3 Filtering of Pole-Like Structure Objects

After detecting vertically continuous objects based on the criteria previously outlined, the next step classifies them as trees or pole structures based on their spatial dispersion in the XY plane (Figure 2). For each detected object, a vertical cylinder is centered at its estimated planimetric position (X_c, Y_c) to isolate the corresponding cluster of points. The 2D Euclidean distances

between (X_c, Y_c) and all points within the cylinder (N) are computed, and the standard deviation (σ_c) of these distances is calculated to quantify the spatial dispersion of the cluster. Objects are classified as trees if $\sigma_c \geq 2 \times s_{grid}$, reflecting the inherent dispersion due to branches and leaves; otherwise, they are considered human-made (e.g., lampposts, traffic signs), which typically have regular cross-sectional shapes ($\sigma_c \approx 0$), resulting in a concentrated point distribution (Equations 2 and 3):

$$Object = \begin{cases} Tree, & \text{if } \sigma_c \geq 2 \times s_{grid} \\ Human - made, & \text{otherwise} \end{cases} \quad (2)$$

where

$$\sigma_c = \sqrt{\frac{1}{N-1} \sum_{i=1}^N (X_i - X_c)^2 + (Y_i - Y_c)^2} \quad (3)$$

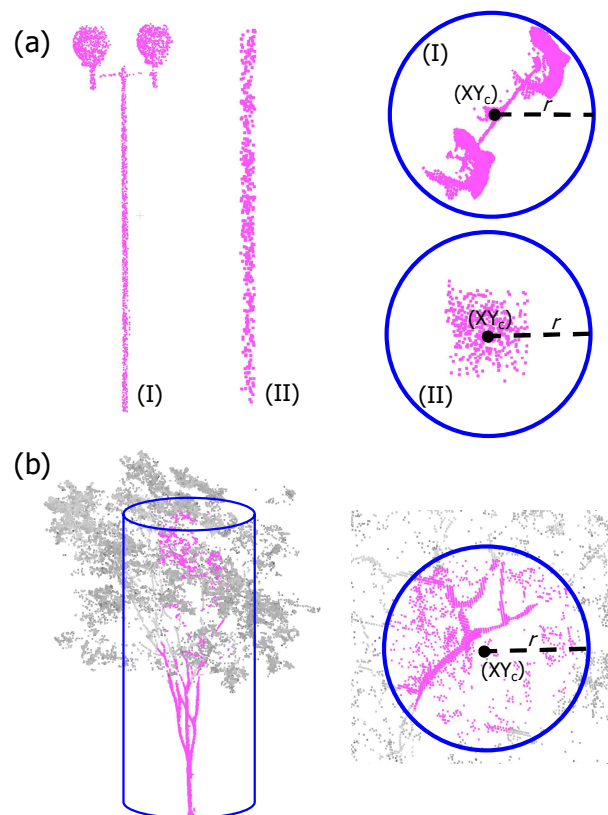


Figure 2. Illustration of object classification using spatial dispersion analysis. (a) Two lampposts (I and II) with their respective top views, showing the cylindrical neighborhood (radius = r , height = starting at $Z_{min} + 0.5$ m to exclude ground points and extending to $+\infty$) and centroid position (XY_c). (b) A tree and its corresponding top view. Points within the cylindrical neighborhood are highlighted in pink.

4. Experimental Design and Quality Assessment

4.1 Backpack LiDAR System

The backpack platform (Figure 3) integrates an Ouster OS0-128 LiDAR sensor (Pacala, 2018), a Dell OptiPlex 3070 microcomputer for data storage, a Ublox GNSS receiver, and a

6S LiPo battery pack for power autonomy. The OS0-128 sensor has a vertical field of view (FoV) of 90° and a horizontal FoV of 360°. The sensor's effective range (at 80% reflectivity) is up to 50 m. It employs a vertical-cavity surface-emitting laser (VCSEL) emitter to generate 128 laser pulses distributed across four vertical columns. This configuration yields a vertical angular resolution of approximately 0.7°. An optical lens assembly directs these pulses to achieve the specified vertical FoV, while a complementary metal-oxide-semiconductor (CMOS) solid-state detector captures the return signals.

The sensor provides a configurable horizontal resolution of 1024 or 2048 points per full rotation and operates at scanning frequencies of 10 or 20 Hz, with a laser wavelength of 865 nm. The emitted beam exhibits a divergence of 0.35° (6.1 mrad) and a diameter of 5 mm, resulting in an overall range accuracy between ±1.5 and 5 cm under varying operational conditions, with an angular precision of ±0.01° in both vertical and horizontal planes. With compact dimensions (85 mm diameter × 73.5 mm height) and a lightweight design (445 g), the sensor is optimized for mobile applications (Castanheiro et al., 2023).

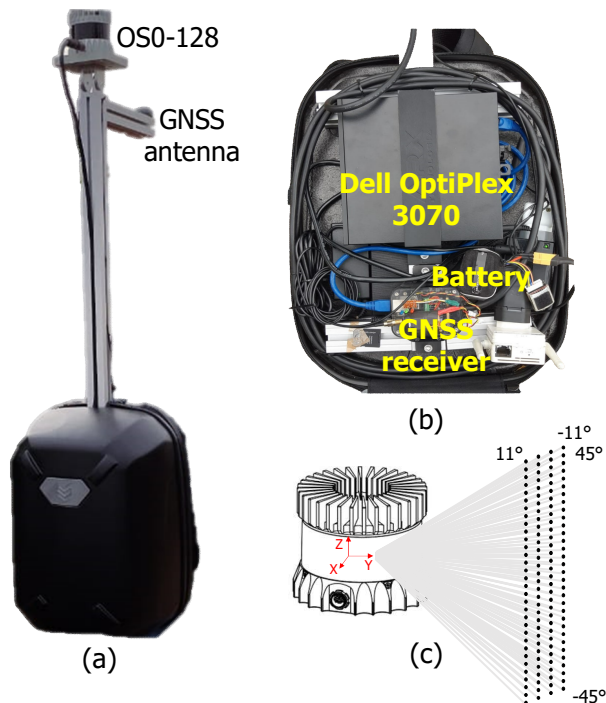


Figure 3. Backpack LiDAR Platform: (a) Backpack and embedded sensors, (b) Onboard computer, battery, GNSS receiver, and WiFi router, and (c) OS0-128 sensor emitting 128 beams simultaneously.

Source: Adapted from Castanheiro et al., 2023.

4.2 Test Areas and Data Acquisition

The experiments were conducted at the São Paulo State University's campus in Presidente Prudente, located in the western region of São Paulo State, Brazil (22°07'21.06" S, 51°23'17.71" W). Three plots with varying levels of complexity and the presence of human-made structures, such as buildings, power poles, lighting poles, tables, benches, and vehicles, were selected to assess the robustness of the proposed tree detection approach (see Figure 4 for a detailed representation of the study area).

The first plot (P₁), covering approximately 90 × 55 m, contains 77 trees, 58 of which are eucalyptus. The second plot (P₂), roughly 105 × 65 m, comprises 49 trees, including coconut palms and other small fruit-bearing species. The third plot (P₃), covering approximately 60 × 40 m, is situated along a road adjacent to a parking lot and contains 30 trees, including yellow Ipê trees. Plots P₁ and P₂ were selected due to their landscaping, which resembles forested and urban green spaces with irregularly distributed trees, some of which are tilted and exhibit diverse shapes and ages. P₃ represents a typical urban scenario, with trees planted along both sides of the road. Additionally, the terrain across all plots is relatively homogeneous.

Data collection was conducted by an operator traversing a predefined close-loop path between trees, beginning and ending at the same control point. This configuration ensures loop closure for optimization of SLAM (Simultaneous Localization and Mapping). The LiDAR sensor operated at 20 Hz with a horizontal angular resolution of 1024 points per complete revolution. Raw point clouds were processed using the Ouster WebSLAM online platform (Ouster, 2021) to align individual scans into a global coordinate system. Metadata recorded for each experimental plot included:

Plot 1: Trajectory length D₁ = 67.03 m, Number of points N₁ = 299.47 million points.

Plot 2: Trajectory length D₂ = 137.29 m, Number of points N₂ = 56.22 million points.

Plot 3: Trajectory length D₃ = 27.3 m, Number of points N₃ = 112.38 million points.

Since the data collection covered large areas, the dataset used in this experiment was subsampled by selecting specific trajectory segments (D₁, D₂, D₃), retaining only the corresponding points.

4.3 Quality Assessment

Qualitative and quantitative analyses were carried out to evaluate the proposed approach's performance. The qualitative assessment involved visually inspecting the detected trees to find inconsistencies and potential omissions compared to manually labeled reference data.

For the quantitative evaluation, three metrics were adopted: completeness, correctness, and F_{Score} (Rutzinger et al., 2009; Sokolova et al., 2006; Wiedemann et al., 1998). These metrics are normalized to a scale from 0 to 1 (or 0% to 100%), with values closer to 1 (100%) indicating a higher degree of concordance between the detection results and the reference data. A planimetric distance threshold was used to determine true positives (T_P), false positives (F_P), and false negatives (F_N). Specifically, a detected tree and its corresponding reference were considered a valid match (i.e., T_P) if the Euclidean distance between their centroids was below a pre-defined threshold. This work's threshold was based on a fixed value (1 m for trunk detection). If there is a double mapping of a tree to the reference, only the closest match is considered. The metrics are defined as follows (Equations 4-6):

$$Completeness = \frac{TP}{TP + FN} \quad (4)$$

$$Correctness = \frac{TP}{TP + FP} \quad (5)$$

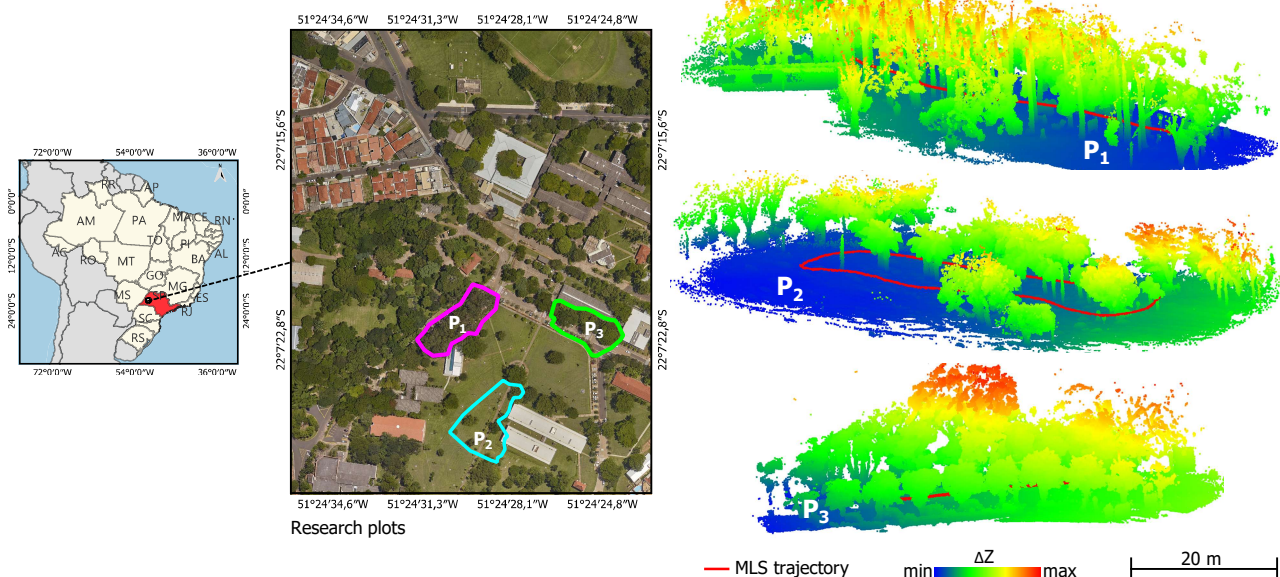


Figure 4. Overview of research plots and corresponding LiDAR point clouds.

$$F_{score} = 2 \times \frac{Completeness \times Correctness}{Completeness + Correctness} \quad (6)$$

where

T_P = Trees labeled in the reference and detected by the approach.

F_N = Trees labeled in the reference but not detected by the approach.

F_P = Trees identified by the approach but not labeled in the reference.

The root mean square error (RMSE) between detected and reference tree positions was also calculated to evaluate tree localization accuracy.

5. Results

Table 1 summarizes the number of reference-labeled trees (R_T), detected trees (D_T), and the counts of true positives (T_P), false positives (F_P), and false negatives (F_N) for each plot. Table 2 presents the individual tree detection quality metrics. Figure 5 shows the results, illustrating the points at the base of the individual trees in green.

Study area	R_T	D_T	T_P	F_N	F_P
Plot 1	77	73	73	4	0
Plot 2	49	48	45	4	0
Plot 3	30	26	25	5	1

Table 1. Detected trees and confusion matrix components (T_P , F_P , F_N) per research plot.

Study area	Quality metrics (%)		
	Completeness	Correctness	F_{Score}
Plot 1	94.8	100	97.3
Plot 2	91.8	100	95.7
Plot 3	83.3	96.2	89.3
Mean	90.0	98.7	94.1

Table 1. Quality metrics for the detection of individual trees.

The positioning errors of the detected tree centers were quantified using RMSE, calculated by comparing the coordinates of the trees manually marked in the point cloud with those extracted by the proposed approach. The specific $RMSE_{XY}$ values for each plot were 27 cm (plot 1), 30.5 cm (plot 2), and 22.8 cm (plot 3), resulting in an average $RMSE_{XY}$ of 26.3 cm.

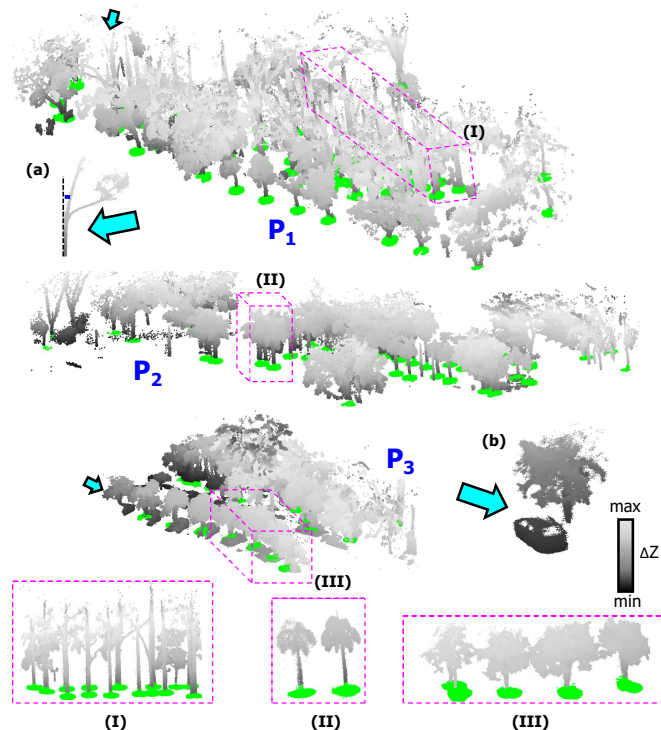


Figure 5. Tree detection results in research plots P_1 , P_2 , and P_3 highlight the identification of different tree species (I, II, III). Items (a) and (b) provide examples of false negatives. Terrain points were excluded to enhance the visibility of tree canopies and the detection of errors.

Furthermore, we analyzed the impact of LiDAR trajectory distance on tree center positioning accuracy. We computed the positional discrepancy (Δ_{XY}) for each detected tree center. Figure 6 displays a scatter plot of these errors as a function of the trajectory distance.

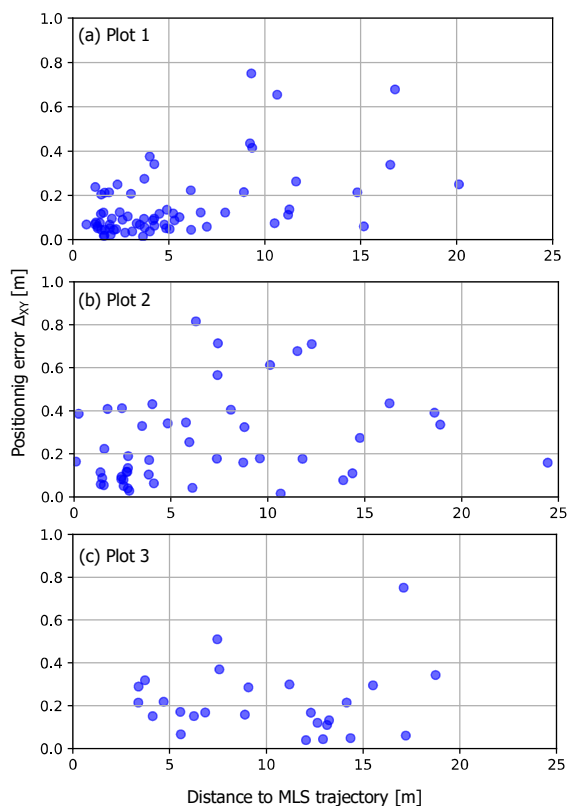


Figure 6. Scatter plot showing positional discrepancies (Δ_{XY}) to proximity to the MLS trajectory.

6. Discussion

The proposed approach showed consistent tree identification across all research plots (Tables 1 and 2), achieving average completeness, correctness, and F_{Score} metrics of 90%, 98.7%, and 94.1%, respectively. This consistency was observed despite species composition and spatial distribution variations across the research plots (Figure 5, I-III). The method relies on four key parameters: B_A , S_{grid} , c_v , and ΔZ .

The B_A parameter filters low-density points that are unlikely to represent trees. In MLS applications, it is well-established that objects of interest tend to be located at close-range distances (Bienert et al., 2021). This distance-based filtering effectively removed points corresponding to facades, buildings, and isolated features. Visual analysis of the raw point clouds indicated that tree canopy features beyond 30 m from the sensor often exhibit significant occlusion or noise due to sensor resolution limitations. Other filtering strategies may also be explored, such as those suggested by Carrilho et al. (2018) and Qin et al. (2018).

The parameters S_{grid} , c_v , and ΔZ characterize the vertical continuity of objects based on the assumption that trees generally grow vertically (Dos Santos, Da Silva, Tommaselli, et al., 2024). S_{grid} and ΔZ are related to minimum object dimensions, whereas c_v is related to the vertical point spacing. In this study, the parameters are set as follows: $S_{grid} = 10$ cm, c_v

$= 10$ cm, and $\Delta Z = 5$ m for plots 1 and 3. For plot 2, which represents an urban forest with shorter trees, ΔZ was set to 3 m.

These parameters are relatively insensitive and require minimal tuning, providing robust baseline settings. For instance, in urban tree mapping, where there are regulatory requirements concerning maximum tree height near urban structures such as powerlines (Bergmann et al., 2024; Carnot et al., 2024; Takahashi & Masuda, 2021; Wanik et al., 2017) or where species-specific information is needed for wood extraction, these parameters are well documented (Kunz et al., 2017).

A pole elimination stage further mitigates false positives. This step utilizes the heuristic observation that trees demonstrate a greater spatial dispersion of branches and leaves than man-made structures, such as poles. We established a threshold of twice the S_{grid} value. This decision reflects our observation that the dispersion of branches and leaves around the estimated center of the tree is generally greater than its diameter. Using a cylindrical neighborhood of 1 m radius and infinite height, the analysis revealed distinct dispersion ranges (s_c): 0.25 - 2.60 m for trees and 0.05 - 0.15 m for poles. This is consistent with previous research (Husain and Vaishya, 2019) that illustrates the utilization of tree crown dimensions to distinguish between natural vegetation and man-made structures.

A false positive occurred in plot 3 despite the pole stage elimination. This occurs due to the presence of an electronic gate situated beneath a tree. The local neighborhood analysis around the estimated centroid incorrectly merged a portion of the tree's branches with the gate due to their proximity. This highlights the limitation of relying solely on cylindrical neighborhoods. Integrating instance segmentation techniques could address this by more accurately delineating object boundaries and preventing such erroneous merging.

Omission errors (false negatives) were noted in all research plots ($P_1 = 4$; $P_2 = 4$; $P_3 = 5$). These errors were due to issues faced during LiDAR sampling, including tilted trees (Figure 5a) and occlusions caused by nearby vehicles (Figure 5b). Trees that are tilted or only partially mapped frequently do not meet the vertical continuity threshold, as occlusion results in a discontinuity in the point cloud representation of the object.

Study plot 3 presented the lowest $RMSE_{XY}$ among all plots (22.8 cm). Given the heterogeneous distribution of trees and their varying proximities to the trajectory throughout the study areas, we investigated the impact of distance from the trajectory on positional error. Within the range of 0 to 25 m, the distance did not significantly affect the magnitude of the positioning error, as no larger errors were observed at the greatest distances. Nevertheless, concerning study plot 2, it was noted that trees identified within the LiDAR trajectory closed path (see Figure 4) demonstrated a 44.13% decrease in error when juxtaposed with those mapped solely on one side of the trajectory. This improvement is attributed to the centroid estimation method, which computes the arithmetic mean of cells classified by an eight-connected region growing algorithm.

7. Conclusions

This study presents an automated method for urban tree detection using rule-based algorithms and the principle of vertical continuity. In addition, a heuristic filter was incorporated to diminish false positives, usually associated with the structural regularity observed in artificial objects. The proposed approach was evaluated using LiDAR point clouds

collected with a backpack LiDAR system. Experiments were conducted across three research plots with varying contextual conditions, yielding a mean F_{Score} of 94.1% and an $RMSE_{XY}$ of 26 cm. By reducing reliance on specific parameters and large labeled datasets, the proposed method offers an efficient and adaptable alternative to classical rule-based and advanced ML/DL-based techniques while facilitating the generation of annotated datasets.

For future work, it is recommended that the proposed approach be evaluated using a more extensive and diverse dataset that includes data from various sources, such as UAV-based LiDAR, terrestrial LiDAR, and photogrammetric point cloud data. Additionally, it is also suggested that the precision of determining central positions for partially sampled or occluded trunks be improved, which is expected to enhance the accuracy of the final position estimates.

Acknowledgments

This study was partly financed by the Coordenação de Aperfeiçoamento de Pessoal de Nível Superior - Brazil (CAPES) – Finance Code 001 and partly by the São Paulo State Research Foundation (FAPESP), Brazil (Process Numbers 2021/06029-7 and 2023/14756-1), and the National Council for Scientific and Technological Development – CNPq (Process Numbers 141550/2020-1 and 309734/2022-3).

References

- Bergmann, M. A., Rodrigues Moreira, L. F., Krohling, B., Silveira, T. L. T., Jung, C. R., Tang, J., Feitosa, M. V., Gomes, R. L. B., & Soares, B. N. (2024). An Approach Based on LiDAR and Spherical Images for Automated Vegetation Inspection in Urban Power Distribution Lines. *IEEE Access*, *12*, 105119–105130. <https://doi.org/10.1109/ACCESS.2024.3431466>
- Bienert, A., Georgi, L., Kunz, M., Von Oheimb, G., & Maas, H.-G. (2021). Automatic extraction and measurement of individual trees from mobile laser scanning point clouds of forests. *Annals of Botany*, *128*(6), 787–804. <https://doi.org/10.1093/aob/mcab087>
- Carnot, M. L., Peukert, E., & Franczyk, B. (2024). Enhancing Roadway Safety: Lidar-Based Tree-Clearance Analysis. *ISPRS Annals of the Photogrammetry, Remote Sensing and Spatial Information Sciences*, *X-4/W4-2024*, 21–28. <https://doi.org/10.5194/isprs-annals-X-4-W4-2024-21-2024>
- Carrilho, A. C., Galo, M., & Santos, R. C. (2018). Statistical outlier detection method for airborne lidar data. *The International Archives of the Photogrammetry, Remote Sensing and Spatial Information Sciences*, *XLII-1*, 87–92. <https://doi.org/10.5194/isprs-archives-XLII-1-87-2018>
- Castanheiro, L. F., Tommaselli, A. M. G., Garcia, T. A. C., Campos, M. B., & Kukko, A. (2023). Point cloud registration using laser data from an orange orchard. *The International Archives of the Photogrammetry, Remote Sensing and Spatial Information Sciences*, *XLVIII-1/W1-2023*, 71–77. <https://doi.org/10.5194/isprs-archives-XLVIII-1-W1-2023-71-2023>
- Da Silva, M. F., dos Santos, R. C., Tommaselli, A. M. G., & Galo, M. (2023). Assessment of Stem Cross-Section Shape and Diameter at Breast Height of Eucalyptus Trees using Terrestrial LiDAR Data. Em *Proceedings of the Brazilian Symposium on Geoinformatics* (p. 210–219). <https://www.scopus.com/inward/record.uri?eid=2-s2.0-85181148798&partnerID=40&md5=d0fa7c952fd9dad53514dc70c78d9bd7>
- Dalla Corte, A. P., Rex, F. E., Almeida, D. R. A. de, Sanquetta, C. R., Silva, C. A., Moura, M. M., Wilkinson, B., Zambrano, A. M. A., Cunha Neto, E. M. da, Veras, H. F. P., Moraes, A. de, Klauber, C., Mohan, M., Cardil, A., & Broadbent, E. N. (2020). Measuring Individual Tree Diameter and Height Using GatorEye High-Density UAV-Lidar in an Integrated Crop-Livestock-Forest System. *Remote Sensing*, *12*(5). <https://doi.org/10.3390/rs12050863>
- Dos Santos, R. C., Da Silva, M. F., Alencar, C. J., & Galo, M. (2024). Automatic Detection of Trees using Airborne LiDAR Data Based on Geometric Characteristics. *ISPRS Annals of the Photogrammetry, Remote Sensing and Spatial Information Sciences*, *X-3-2024*, 109–115. <https://doi.org/10.5194/isprs-annals-X-3-2024-109-2024>
- Dos Santos, R. C., Da Silva, M. F., Tommaselli, A. M. G., & Galo, M. (2024). Automatic Tree Detection/Localization in Urban Forest Using Terrestrial Lidar Data. *IGARSS 2024 - 2024 IEEE International Geoscience and Remote Sensing Symposium*, 4522–4525. <https://doi.org/10.1109/IGARSS53475.2024.10642701>
- Hu, T., Wei, D., Su, Y., Wang, X., Zhang, J., Sun, X., Liu, Y., & Guo, Q. (2022). Quantifying the shape of urban street trees and evaluating its influence on their aesthetic functions based on mobile lidar data. *ISPRS Journal of Photogrammetry and Remote Sensing*, *184*, 203–214. <https://doi.org/10.1016/j.isprsjprs.2022.01.002>
- Hui, Z., Li, Z., Jin, S., Liu, B., & Li, D. (2022). Street Tree Extraction and Segmentation from Mobile LiDAR Point Clouds Based on Spatial Geometric Features of Object Primitives. *Forests*, *13*(8), 1245. <https://doi.org/10.3390/f13081245>
- Husain, A., & Vaishya, R. C. (2019). Detection and thinning of street trees for calculation of morphological parameters using mobile laser scanner data. *Remote Sensing Applications: Society and Environment*, *13*, 375–388. <https://doi.org/10.1016/j.rsase.2018.12.007>
- Kou, Y., Gao, X., Zhang, Y., Liu, T., An, G., Ye, F., Tian, Y., & Chen, Y. (2025). Hierarchical Optimization Segmentation and Parameter Extraction of Street Trees Based on Topology Checking and Boundary Analysis from LiDAR Point Clouds. *Sensors*, *25*(1), 188. <https://doi.org/10.3390/s25010188>
- Kulicki, M., Cabo, C., Trzcinski, T., Będkowski, J., & Stereńczak, K. (2024). Artificial Intelligence and Terrestrial Point Clouds for Forest Monitoring. *Current Forestry Reports*, *11*(1), 5. <https://doi.org/10.1007/s40725-024-00234-4>
- Kunz, M., Hess, C., Raunonen, P., Bienert, A., Hackenberg, J., Maas, H., Härdtle, W., Fichtner, A., & Von Oheimb, G. (2017). Comparison of wood volume estimates of young trees from terrestrial laser scan data. *iForest - Biogeosciences and Forestry*, *10*(2), 451–458. <https://doi.org/10.3832/ifer2151-010>
- Lee, C., Park, A. H., Lee, H., Bratman, G. N., Hankey, S., & Li, D. (2024). Measuring urban nature for pedestrian health: Systematic review and expert survey. *Landscape and Urban*

- Planning, 250, 105129. <https://doi.org/10.1016/j.landurbplan.2024.105129>
- Luo, H., Khoshelham, K., Chen, C., & He, H. (2021). Individual tree extraction from urban mobile laser scanning point clouds using deep pointwise direction embedding. *ISPRS Journal of Photogrammetry and Remote Sensing*, 175, 326–339. <https://doi.org/10.1016/j.isprsjprs.2021.03.002>
- Ma, S., Chen, Y., Li, Z., Chen, J., & Zhong, X. (2025). Improved Cylinder-Based Tree Trunk Detection in LiDAR Point Clouds for Forestry Applications. *Sensors*, 25(3), 714. <https://doi.org/10.3390/s25030714>
- Neyns, R., & Canters, F. (2022). Mapping of Urban Vegetation with High-Resolution Remote Sensing: A Review. *Remote Sensing*, 14(4), 1031. <https://doi.org/10.3390/rs14041031>
- Ouster. (2021). *Web SLAM*. <https://webslam.ouster.dev/>
- Pacala, A. (2018, novembro 8). *How Multi-Beam Flash LiDAR Works*. <https://ouster.com/insights/blog/how-multi-beam-flash-lidar-works>
- Qin, H., Guan, G., Yu, Y., & Zhong, L. (2018). A voxel-based filtering algorithm for mobile LiDAR data. *The International Archives of the Photogrammetry, Remote Sensing and Spatial Information Sciences*, XLII-3, 1433–1438. <https://doi.org/10.5194/isprs-archives-XLII-3-1433-2018>
- Rutzinger, M., Rottensteiner, F., & Pfeifer, N. (2009). A Comparison of Evaluation Techniques for Building Extraction From Airborne Laser Scanning. *IEEE Journal of Selected Topics in Applied Earth Observations and Remote Sensing*, 2(1), 11–20. <https://doi.org/10.1109/JSTARS.2009.2012488>
- Shao, J., Zhang, W., Mellado, N., Wang, N., Jin, S., Cai, S., Luo, L., Lejemble, T., & Yan, G. (2020). SLAM-aided forest plot mapping combining terrestrial and mobile laser scanning. *ISPRS Journal of Photogrammetry and Remote Sensing*, 163, 214–230. <https://doi.org/10.1016/j.isprsjprs.2020.03.008>
- Sokolova, M., Japkowicz, N., & Szpakowicz, S. (2006). Beyond Accuracy, F-Score and ROC: A Family of Discriminant Measures for Performance Evaluation. In A. Sattar, B. Kang, O. Nierstrasz, T. Kanade, J. Kittler, J. M. Kleinberg, F. Mattern, J. C. Mitchell, M. Naor, D. Hutchison, C. Pandu Rangan, B. Steffen, M. Sudan, D. Terzopoulos, D. Tygar, M. Y. Vardi, & G. Weikum (Eds.), *AI 2006: Advances in Artificial Intelligence* (Vol. 4304, p. 1015–1021). Springer Berlin Heidelberg. http://link.springer.com/10.1007/11941439_114
- Solares-Canal, A., Alonso, L., Picos, J., & Armesto, J. (2023). Automatic tree detection and attribute characterization using portable terrestrial lidar. *Trees*, 37(3), 963–979. <https://doi.org/10.1007/s00468-023-02399-0>
- Takahashi, G., & Masuda, H. (2021). Roadside tree extraction and diameter estimation with MMS LiDAR by using point-cloud image. *ISPRS Annals of the Photogrammetry, Remote Sensing and Spatial Information Sciences*, V-2–2021, 67–74. <https://doi.org/10.5194/isprs-annals-V-2-2021-67-2021>
- Wang, Y., Jiang, T., Liu, J., Li, X., & Liang, C. (2020). Hierarchical Instance Recognition of Individual Roadside Trees in Environmentally Complex Urban Areas from UAV Laser Scanning Point Clouds. *ISPRS International Journal of Geo-Information*, 9(10), 595. <https://doi.org/10.3390/ijgi9100595>
- Wanik, D. W., Parent, J. R., Anagnostou, E. N., & Hartman, B. M. (2017). Using vegetation management and LiDAR-derived tree height data to improve outage predictions for electric utilities. *Electric Power Systems Research*, 146, 236–245. <https://doi.org/10.1016/j.epr.2017.01.039>
- Wiedemann, C., Heipke, C., Mayer, H., Jamet, O., 1998. Empirical evaluation of automatically extracted road axes. In K. W. Bowyer and P. J. Phillips (Eds.), *Empirical evaluation techniques in computer vision* (pp. 172–187). Wiley-IEEE Computer Society Press.
- Wu, R., Chen, Y., Wang, C., & Li, J. (2018). Estimation of Forest Trees Diameter from Terrestrial Laser Scanning Point Clouds Based on a Circle Fitting Method. *IGARSS 2018 - 2018 IEEE International Geoscience and Remote Sensing Symposium*, 2813–2816. <https://doi.org/10.1109/IGARSS.2018.8517303>
- Yang, J., Gan, R., Luo, B., Wang, A., Shi, S., & Du, L. (2024). An Improved Method for Individual Tree Segmentation in Complex Urban Scenes Based on Using Multispectral LiDAR by Deep Learning. *IEEE Journal of Selected Topics in Applied Earth Observations and Remote Sensing*, 17, 6561–6576. <https://doi.org/10.1109/JSTARS.2024.3373395>
- Yao, W., Krull, J., Krzystek, P., & Heurich, M. (2014). Sensitivity Analysis of 3D Individual Tree Detection from LiDAR Point Clouds of Temperate Forests. *Forests*, 5(6), 1122–1142. <https://doi.org/10.3390/f5061122>